IOP PUBLISHING JOURNAL OF MICROMECHANICS AND MICROENGINEERING

J. Micromech. Microeng. **18** (2008) 045024 (7pp) doi:10.1088/0960-1317/18/4/045024

Buckled cantilevers for out-of-plane platforms

R W Johnstone, A H Ma, D Sameoto, M Parameswaran and A M Leung

Institute For Micromachine and Microfabrication Research, School of Engineering Science, Simon Fraser University, 8888 University Dr, Burnaby, British Columbia V5A 1S6, Canada

E-mail: rjohnsto@sfu.ca

Received 4 January 2008, in final form 8 February 2008
Published 14 March 2008
Online at stacks.iop.org/JMM/18/045024

Abstract

In this paper, we show how surface-micromachined buckled cantilevers can be used to construct out-of-plane structures. We include the relevant theory necessary to predict the height and angle of plates attached to buckled cantilevers, as well as the mechanical stresses involved in assembly. These platforms can be assembled to any angle between 0° and 90° with respect to the substrate by changing the attachment point and the amount of deflection. Example devices were fabricated using PolyMUMPs™ and assembled. Using these devices, the deflection of the buckled cantilevers was verified, as well as the placement for raised platforms.

1. Introduction

Since the seminal paper on surface-micromachined hinges [1], many interesting designs for out-of-plane structures have been presented. Examples of applications exist, for example, in free-space optics [2–4] and RF systems [5]. Out-of-plane structures are important because they free systems from the constraints of planar processing. Unfortunately, effective methods of assembling these structures after release impose additional demands on the fabrication process. A wide variety of mechanisms have been suggested to achieve the post-release assembly. These include on-chip mechanisms [6, 7], which consume significant on-chip real estate, and specialized off-chip mechanisms [8–13]. Techniques have also been developed to take advantage of micro-scale phenomena, such as thermal kinetic assembly [14], surface tension [15–19] and non-uniform residual stresses [20–23].

However, as with many other sliding contact systems, researchers have also investigated out-of-plane assembly techniques that eliminate staple hinges. For example, surface tension mediated assembly can be accomplished without mechanical hinges [19]. Some of the previously mentioned techniques can be combined with compliant hinges. Combining non-uniform stress assembly with compliant mechanisms leads to micro-origami [20, 21]. Combining off-chip mechanisms with compliant mechanisms leads to nonlinear suspensions [11–13]. Additionally, unlike sliding contact hinges, compliant hinges can often be fabricated using a single free-standing layer, making them useful in many microfabrication processes that do not support staple hinges.

In particular, Tsang *et al* [11–13] have developed a compliant suspension for use in assembling 90° out-of-plane structures. This design uses off-chip mechanical actuation to complete the assembly after release, but the assembly process is particularly simple, and can be accomplished with a single push. This design thus achieves out-of-plane structures while imposing minimal additional fabrication complexity. However, Tsang-suspensions really only handle 90° structures. Thermal isolation platforms, which are parallel to the substrate, can be fabricated using two Tsang-suspensions, but this then loses the simple assembly process.

In this paper, we present a compliant device capable of assembling off-chip platforms parallel to the substrate surface with a single push. Additionally, the platforms can be set to an orientation anywhere in a continuous range of from 0° to 90° with respect to the substrate. This is accomplished by using a buckled cantilever [24, 25]. The cantilever is buckled using a single mechanical push, and afterwards is constrained from relaxing by a mechanical stop (figure 1). Depending on where along the cantilever the platform is attached, the angle can be controlled. Additionally, since the cantilever is connected to the substrate through a compliant connection, electrical connections can be readily routed to the platform.

In addition to the simplicity of assembly, buckled cantilevers can be fabricated in any surface-micromachining process with a single free-standing layer. So far,

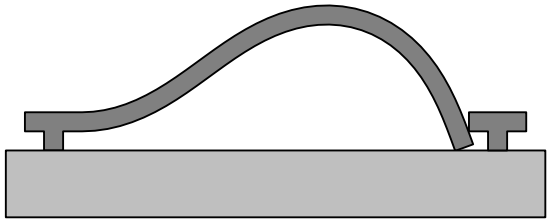

Figure 1. Illustration of a buckled cantilever. The cantilever is anchored on the left. On the right, the cantilever's tip is hooked behind a mechanical stop. This configuration forms a fixed-hinged beam.

implementations have been shown in SU-8 [25], polyimide and polysilicon.

2. Theory

2.1. Linear solution

An illustration of a buckled cantilever is shown in figure 1. As one can see, the structure is quite simple and consists of the cantilever itself along with a mechanical stop. The left end of the cantilever is constrained so that both its deflection and slope are fixed, while for right end, only the position is fixed. The cantilever can thus be modelled as a fixed-hinged beam. Using linear beam-bending theory, one can determine the buckling load and mode-shape of the buckled cantilever [26].

First, the critical force necessary to induce buckling is [26]

$$P_{\mathrm{cr}} = \frac{\pi^2 E I}{L_{\mathrm{eff}}^2} = \frac{\pi^2 E I}{(0.6992L)^2}. \tag{1}$$

Above, P_{cr} is the critical force, E is the modulus of elasticity for the cantilever material, I is the bending moment of inertia for the cantilever, and L_{eff} is the effective length of the cantilever. The effective length of the beam is related to the actual cantilever length, but corrected to account for the boundary conditions. In the case of a fixed-hinged beam, $L_{\mathrm{eff}} = 0.6992L$, where L is the cantilever's actual length.

The mode-shape for the buckled cantilever is [26]

$$w(x) = \sin(kx) - kL\cos(kx) + kL\left(1 - \frac{x}{L}\right). \tag{2}$$

In equation (2), $w(x)$ is the transverse deflection of the cantilever, x is the position along the cantilever with $x = 0$ being the fixed end, and $k = 1.4303\pi/L$. This mode shape is illustrated in figure 2. Note, $w(x)$ is an eigenfunction, and so only specifies the shape of the deflection. It cannot be used to calculate the magnitude of the deflection. However, this is sufficient to find the location of key points of interest, if not their associated values. For our particular application, there are three points that we would like to locate: the highest point along the cantilever, the point of maximum stress, and any points of no stress.

Finding the first point, the point of maximum height, is a simple question of finding the extrema of the mode-shape.

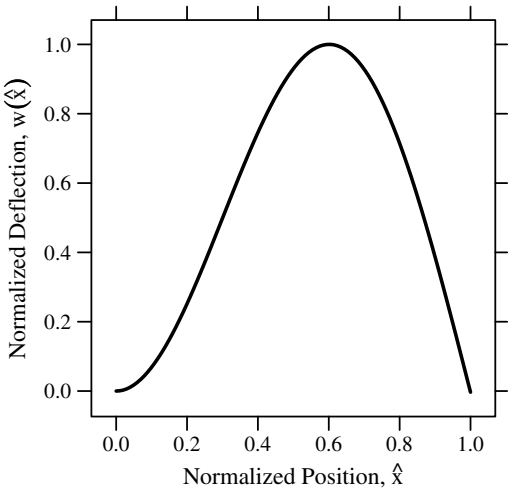

Figure 2. Plot of the mode-shape for buckled fixed-hinged beams. The normalized distance is $\hat{x} = x/L$.

From figure 2, one can exclude the end-points of the function. Thus the problem reduces to solving $w'(x) = 0$, which has two solutions. One solution is the already discarded case of $x = 0$, and the second solution is $x = 0.6017L$. Thus, to first order, attaching a platform to the buckled cantilever at a position 60.17% along its length will provide the maximum height. Also, since the slope of the cantilever is zero at this point, the attached platform will be parallel to the substrate.

The second point of interest is the point of maximum stress in the beam. This point can be located by first noting that the stress is related bending moment as follows:

$$\begin{aligned}\sigma_{\max}(x) &= \frac{c}{I}|M(x)| \\ &= \frac{c}{I}\left|-EI\frac{\mathrm{d}^2 w(x)}{\mathrm{d}x^2}\right| \\ &= Ec\left|\frac{\mathrm{d}^2 w(x)}{\mathrm{d}x^2}\right|.\end{aligned} \tag{3}$$

Equation (3) can be considered, in a sense, a mode-shape for the stress profile for the cantilever. In this equation, we have introduced $M(x)$, the bending moment, and c, the maximum fibre distance. For a cantilever with a rectangular cross-section, $c = t/2$, where t is the cantilever's thickness.

Using equation (3), one can calculate the maximum stress in a cross-section anywhere along the beam. However, we are interested in finding the point of maximum stress overall, $\sigma_{\max}$. We thus want to find the extrema of the second derivative. The point of maximum stress is located at $x = 0.6504L$.

Finally, we note that there is a point where the bending moment is zero, located at $x = 0.3008L$. This point might be the preferred attachment point for any devices that would be adversely affected by stress. However, as will be shown later, other options for relatively stress-free attachment exist that could give more height, as well as place the device parallel to the substrate.

Before continuing, it should be noted that the position of the three points located are only valid to first order. A numerical solution, which does not use the paraxial

approximation, will be presented next. This nonlinear approach not only corrects for some small errors in the positions already located, but can also provide values for the maximum height and the maximum stress.

2.2. Nonlinear solution

Determining a relationship between the applied load and the cantilever's deflection is considerably more complicated when the paraxial approximation is dropped. Solving the solution requires a change in perspective, and instead the beam's position is determined as a function of the position along the cantilever, s. Somewhat reasonable close-form solutions involving elliptic integrals are available to determine the deflection from the load and the cantilever's material and geometric parameters [27]. However, we would like to specify the deflection of the tip, and then determine the load. Furthermore, we would like to determine the complete displacement profile to determine the maximum height, the position of maximum height, and other points of interest. We have therefore resorted to a numerical solution.

To solve for the beam's deflection profile, we start by assuming an end load. The moment at all positions along the cantilever can be readily determined from the following formula:

$$M(s) = [a - x(s)]P\sin\phi - [b - y(s)]P\cos\phi + M_0. \tag{4}$$

In equation (4), $M(s)$ is the moment at a distance s along the cantilever, a and b are the target horizontal and vertical coordinates for the position of the cantilever's end, $x(s)$ and $y(s)$ are the coordinates of the element of the cantilever currently under consideration, P is the magnitude of the applied force, and ϕ is the angle between the applied force and the negative x-axis, and M_0 is a moment applied to the end of the cantilever. However, for this application, $M_0 = 0$ as there is no applied moment.

The sign conventions for the force magnitude and direction in equation (4) are set for positive axially applied forces. A positive value for P with $\phi = 0$ implies an axially applied compressive force.

The deflection profile of the cantilever can be specified in terms of a nonlinear boundary value problem (BVP). However, the BVP was solved using a method somewhat analogous to the shooting method, and so the BVP was reduced to an initial value problem. This formulation specifies the configuration of each differential segment of the cantilever by its position and angle. A system of ordinary differential equations describing the cantilevers deflection is [27]

$$\begin{aligned}\frac{\mathrm{d}\theta(s)}{\mathrm{d}s} &= \frac{M(s)}{EI}\\ \frac{\mathrm{d}x(s)}{\mathrm{d}s} &= \cos\theta(s)\\ \frac{\mathrm{d}y(s)}{\mathrm{d}s} &= \sin\theta(s).\end{aligned} \tag{5}$$

The initial value problem also has the following initial conditions. The initial conditions are derived from the boundary conditions on the fixed-end of the cantilever, which are the known position and orientation of the cantilever's anchor:

$$\begin{aligned}\theta(s)|_{s=0} &= 0\\ x(s)|_{s=0} &= 0\\ y(s)|_{s=0} &= 0.\end{aligned} \tag{6}$$

The problem description also includes two other conditions, $x(s)|_{s=L} = a$ and $y(s)|_{s=L} = b$. These are the target for the shooting method and correspond to the boundary conditions on the hinged-end of the cantilever. These conditions ensure that the cantilever's end is actually at the position where the applied force was specified. The two conditions at $s = L$ are not enforced by the initial value problem specified in equations (5) and (6). This will be handled later.

To ease analysis, we have converted the initial value problem to a non-dimensional form. We have also substituted equation (4) into equation (5). This results in the following system:

$$\begin{aligned}\frac{\mathrm{d}\theta(\hat{s})}{\mathrm{d}\hat{s}} &= \{[\hat{a} - \hat{x}(\hat{s})]\sin\phi - [\hat{b} - \hat{y}(\hat{s})]\cos\phi + \eta\}\gamma\\ \frac{\mathrm{d}\hat{x}(\hat{s})}{\mathrm{d}\hat{s}} &= \cos\theta(\hat{s})\\ \frac{\mathrm{d}\hat{y}(\hat{s})}{\mathrm{d}\hat{s}} &= \sin\theta(\hat{s}).\end{aligned} \tag{7}$$

In equation (7), the variables with a hat are simply normalized versions of the variables from equation (5). For example, $\hat{a} = a/L$. Two new non-dimensional variables have been added, which are the normalized moment, $\eta = M_0/PL$, and the normalized force, $\gamma = PL^2/EI$. Again, η is being included for completeness, although it will be zero in this application. Solving the system of differential equations specified by equation (7) is a simple numerical problem, except for enforcing the constraints on the beam end. To overcome this problem, we used a nonlinear minimization to find the values of P and ϕ such that the deflection of the cantilever end, as predicted by the system of differential equations, matches the target values of $\hat{a}$ and $\hat{b}$. The nonlinear minimization used the sum of the squared errors for P and ϕ as the fitness function. Furthermore, the fitness function was minimized using the coordinate descent method [28].

Solving the system specified by equation (7) not only provides the deflection profile of the cantilever, but can also be used to readily determine the bending stresses along the length of the cantilever. However, typically only the maximum stress is of interest [27]:

$$\begin{aligned}\sigma_{\max} &= \frac{c}{I}|M(s)|_{\max}\\ &= \frac{c}{I}\left|EI\frac{\mathrm{d}\theta(s)}{\mathrm{d}s}\right|_{\max}\\ &= \frac{Ec}{L}\hat{\sigma}_{\max}.\end{aligned} \tag{8}$$

Where we have defined the non-dimensional maximum stress, $\hat{\sigma}_{\max}$, as follows:

$$\hat{\sigma}_{\max} \equiv \left|\frac{\mathrm{d}\theta(\hat{s})}{\mathrm{d}\hat{s}}\right|_{\max}. \tag{9}$$

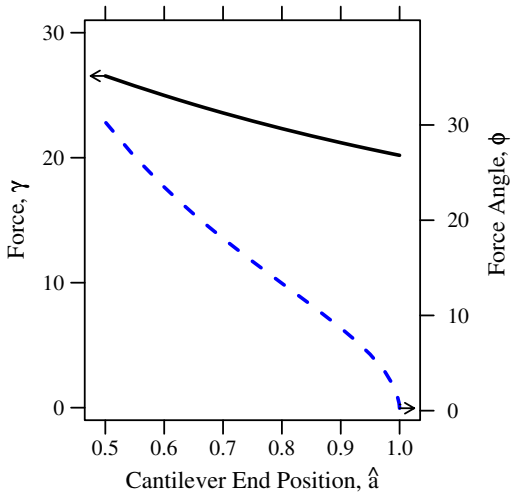

Figure 3. Plot of the non-dimensional force and the force angle necessary to buckle the cantilever back to a specified position.

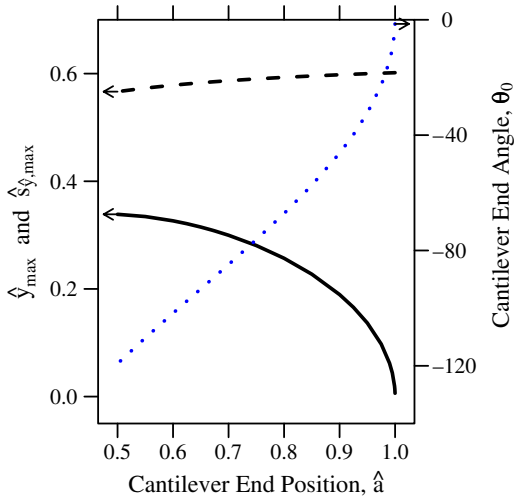

Figure 4. Plot of the maximum non-dimensional height (solid), the position along the cantilever where the maximum deflection occurs (dashed), and the angle of the cantilever end.

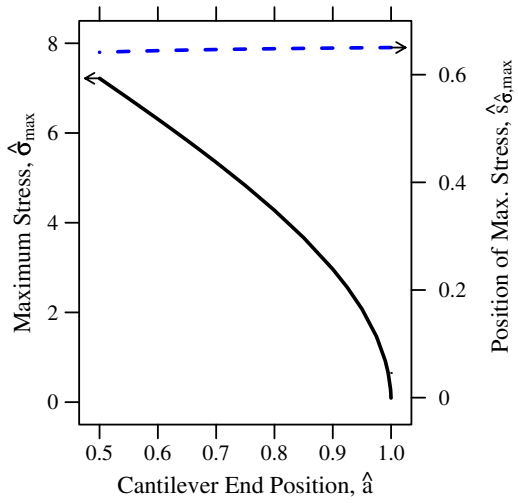

Figure 5. Plot of the maximum non-dimensional stress and the position along the cantilever where the maximum stress occurs.

The non-dimensional maximum stress is readily extracted from the numerical solution. One can then use equation (8) to work out the actual maximum stress.

Using the above mathematics, we have calculated the parameters for values of $\hat{a}$ from 0.5 to 1. Clearly, $\hat{a} = 1$ is the maximum value possible. The value of $\hat{a} = 0.5$ as the minimum is somewhat arbitrary, as the cantilever could, in principle, be deflected further. However, the results indicate that even deflecting the cantilever back to this value is not practical, as the angle of cantilever's tip is already greater than 90° at this point. In all of these simulations, $\hat{b} = 0$, implying no vertical displacement of the tip. In reality, because of the design of the mechanical stop, the tip will see a small downward deflection (see figure 1). However, this would typically only be a small correction, and is neglected in the plots that follow.

First of interest is the non-dimensional force, shown in figure 3. As expected, the required force, γ, is a minimum for the smallest deflections, which correspond to the largest values of $\hat{a}$. This minimum should be less than 20.2, which was calculated for $\hat{a} = 0.999$. Referring back to equation (1), one can make a predication of γ by simple rearrangement. This gives a value for $\gamma = 20.19$, showing good agreement for small deflections.

Second, moving to the nonlinear solution has provided a numerical value for the maximum height of the cantilever, shown in figure 4. Additionally, the position of the maximum height is shown. The linear model predicts that the position of maximum height should be $\hat{s} = 0.6017$. Again, this agrees very well with the nonlinear model as $\hat{a} \to 1$, but the nonlinear model also shows corrections as $\hat{a}$ is varied.

Figure 4 also plots the angle of the cantilever end as $\hat{a}$ is varied. As expected, the angle approaches zero as $\hat{a} \to 1$. An important transition occurs at $\hat{a} = 0.6697$. At this value, the angle of the cantilever's tip is equal to 90°. Thus, for example, if one wanted to assemble plates so that they were oriented at 90°, those plates could be attached to the cantilever's tip. While the cantilever can be deflected further, the angle will continue to increase, reducing the effectiveness of the mechanical stop.

The maximum stress is plotted in figure 5. The position of the maximum stress, $\hat{s}_{\hat{\sigma},\max}$ again shows very good agreement as $\hat{a} \to 1$. The numerical solution reaches 0.650, which matches the linear model.

3. Failure prior to buckling

In addition to failure from the bending stresses, cantilevers may fail prior to buckling. This can occur if the cantilever cannot withstand the critical axial stress necessary to induce buckling. Modifying equation (1) to find the critical stress instead of the critical force, one finds that

$$\sigma_{cr} = \frac{\pi^2 E h^2}{12 L_{\text{eff}}^2} = \frac{\pi^2 E c^2}{3 L_{\text{eff}}^2}. \tag{10}$$

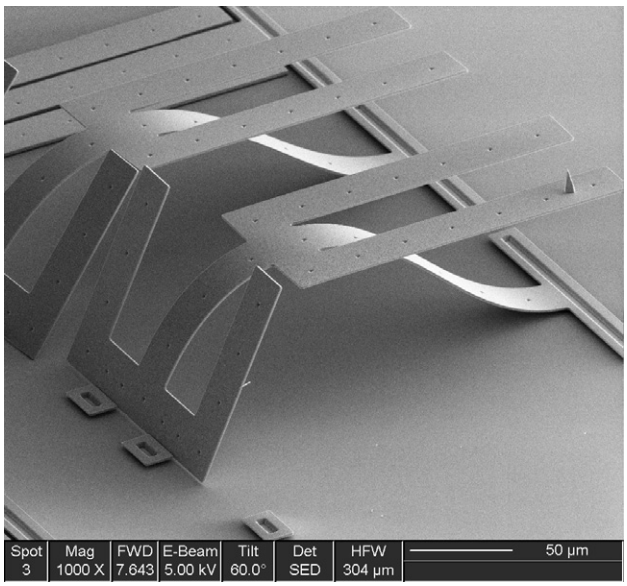

Figure 6. SEM of an assembled buckled cantilever fabricated in polysilicon. This cantilever was fabricated in the POLY2 layer of PolyMUMPs™ The cantilever has a length of 300 μm a width of 30 μm and a thickness of 1.5 μm. The mechanical stops are set at $\hat{a} = 0.8$. One of the parallel platforms is supporting a piece of debris from a nearby cantilever that failed during assembly.

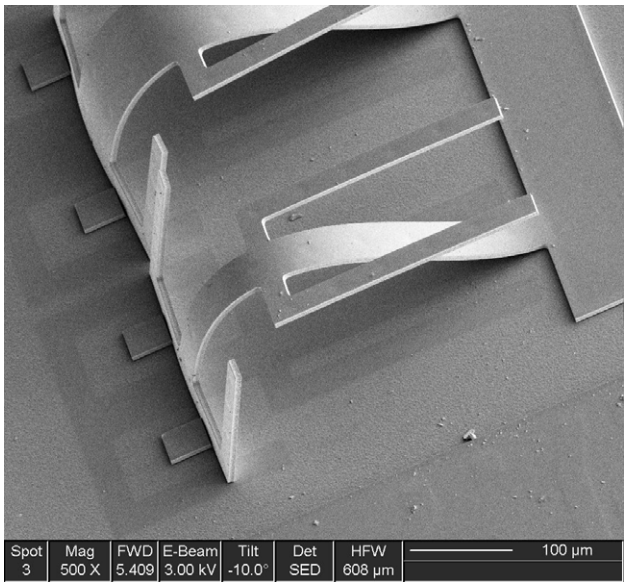

Figure 7. SEM of an assembled buckled cantilever fabricated in polyimide. This cantilever was fabricated using an in-house process. The cantilever has a length of 500 μm a width of 50 μm and a thickness of 7.3 μm. The mechanical stops are set at $\hat{a} = 0.67$.

Comparing equation (10), for the critical buckling stress, to equation (8), for maximum stress after bending, one should note different scaling based on the geometric parameters. In particular, shorter thicker cantilevers may fail prior to buckling, even if they could withstanding the bending stresses in their final configuration. This is especially true as $\hat{a} \to 1$, as the bending stress goes to zero while the critical buckling stress remains fixed.

Although not seen in the PolyMUMPs™ cantilevers discussed later, this was noted as an important failure mode for earlier SU-8 cantilevers [25].

4. Experiment

To confirm the design and theory of buckled cantilevers, several implementations were fabricated using PolyMUMPs™ [29]. An example of a assembled cantilever is shown in figure 6. Previous work has shown buckled cantilevers fabricated using SU-8 [25], and we have also successfully assembled buckled cantilevers fabricated in polyimide (figure 7). Buckled cantilevers were fabricated in both POLY1 and POLY2, with lengths of 100 μm 200 μm and 300 μm. For each length, various values of $\hat{a}$ between 0.65 and 0.85 were fabricated. For this work, the cantilevers were assembled manually using a micropositioner. The buckled cantilevers all have two pairs of beams.

- Each buckled cantilever has a pair of beams attached partway down their length that are positioned, according to the calculations in section 2.2, at the position of maximum height. These beams should also be parallel with the substrate. The beams are extended so that their plane may be compared against the substrate to double-check that they are indeed parallel.
- Each buckled cantilever also has a pair of beams attached at the cantilever tip. Again, the purpose of these beams is to allow for their orientation to be extracted. The angle of the cantilever tip can thus be compared against predictions.

The lengths chosen for the buckled cantilevers were unfortunately chosen based on initial, incorrect calculations, which underestimated the necessary bending stresses. Corrected values show that, for the material and thicknesses in PolyMUMPs™ these cantilevers are too short, and subject to unsafe stresses. While all of the cantilevers could be buckled, most of the designs could not be deflected sufficiently to engage the mechanical stops. The corrected bending stress predications are shown in table 1 for a subset of the values of $\hat{a}$ fabricated.

While the fracture statistics of micro-scale structures is subject to significant statistical variation [30], the POLY2 layer of the PolyMUMPs™ process has a measured yield strength of 1.51 $\pm$ 0.26 GPa [31]. This is in good agreement with our ability to assemble these structures. Nearly all of the buckled cantilevers with $L = 300$ μm and $\hat{a} = 0.85$ were assembled, while only a few cantilevers with $L = 300$ μm and $\hat{a} = 0.8$ were assembled successfully. No buckled cantilever with other geometric parameters, in either POLY1 or POLY2, were successfully assembled.

For POLY1, the agreement is nearly as good. The reported strength of POLY1 is 1.67 $\pm$ 0.23 GPa. This would indicate that some of the longest POLY1 buckled cantilever should have been able to withstand the buckling stresses, which is not the case. However, the value is borderline, and the failure

Table 1. Predicted maximum bending stresses for buckled cantilevers at the fabricated lengths for a subset of $\hat{a}$. The difference in the maximum bending stress in POLY1 and POLY2 is due to their different thicknesses, at 2.0 μm and 1.5 μm, respectively.

Length (μm)	POLY1 (GPa)			POLY2 (GPa)		
	$\hat{a} = 0.75$	$\hat{a} = 0.8$	$\hat{a} = 0.85$	$\hat{a} = 0.75$	$\hat{a} = 0.8$	$\hat{a} = 0.85$
100	7.6	6.8	5.8	5.7	5.1	4.3
200	3.8	3.4	2.9	2.9	2.5	2.2
300	2.5	2.3	1.9	1.9	1.7	1.4

could easily result in difference in the mechanical properties between fabrication runs.

Furthermore, for both POLY1 and POLY2, assembly requires that the cantilever be deflected past the mechanical stop. This obviously requires the cantilever's to endure transient stresses in excess of those listed in table 1. This over-stress is further compounded when the applied force is not aligned axially, leading to additional torsional stresses on the cantilever.

Many of the failures also occurred at the cantilever's anchor, instead of near $\hat{s} = 0.65$ as expected. While that is the point of maximum stress, the stress at the cantilever's anchor is not much less. For example, at $\hat{a} = 0.85$, the maximum non-dimensional stress is 3.67 while the non-dimensional stress at the anchor is 3.55. The bending stress at the anchor is thus nearly as large as the maximum stress. When this stress is combined either with thinner polysilicon films on sidewalls or with the stress concentration at the corner, the anchor becomes the point of failure.

Not clear from figure 6, most of the mechanical stops were damaged during assembly. This was not a problem with the design of the mechanical stops per se, but the small gap between the stops, which left insufficient room for the passage of the micropositioner's tip.

Using optical microscopy, the height of the parallel platforms connected to several of the successfully assembled cantilevers were measured. For the $\hat{a} = 0.85$ cantilevers, the height was measured at 64 ± 3 μm. This compares to the predicted value of 68.22 μm. However, correcting for the small downward deflection caused by the mechanical stop, $\hat{b} = -0.014$, leads to a more accurate prediction of 65.69 μm. Measurements of a $\hat{a} = 0.8$ cantilever determined the height of the platform to be 70 ± 2 μm high. With the correction for $\hat{b}$, the predicted height is 74.50 μm.

For cantilevers with $\hat{a} = 0.85$, the tip angles were measured to be $52 \pm 1^\circ$. This compares to a predicted tip angle of 57°.

Although the first measurement is within error, both height measurements are below their corresponding predictions. There is an additional discrepancy in the cantilevers tip angles. These differences are likely due to a non-ideality of the device shown in figure 6, which is that the connection for the platforms is 25 μm wide, stiffening that portion of the cantilever. In total, slightly less than 17% of the cantilever is stiffened because of the attached platforms. This flattens the top portion of the cantilever, thus lowering the maximum height. This could be corrected by using a smaller connection between the platforms and the cantilever.

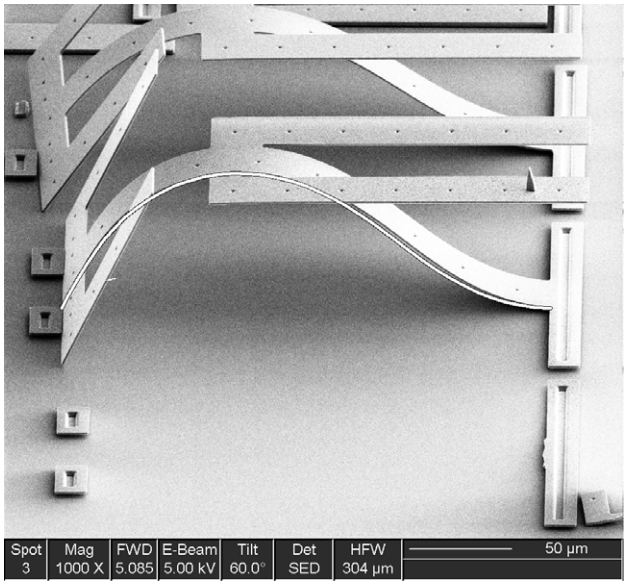

Figure 8. SEM of a buckled cantilever with the predicted cantilever shaper super-imposed. Predicted shape was superimposed using an affine transformation.

The shape that the cantilevers follow matches closely the predicted paths. An example is shown in figure 8. The superimposed shape contains some inaccuracy, as the mapped path does not correct for the vanishing perspective of the SEM. While the match is relatively good, there are deviations. These deviations are due to the additional stiffness created by the wide connections to the two pairs of attached platforms. The influence of the platforms parallel to the substrate could be minimized by moving to narrower connections, although that might not be possible if those connections must carry electrical interconnects.

5. Summary

In this paper, we have shown how the shape of a buckled cantilever can be determined. Plates can be attached to these cantilevers to create various types of out-of-plane structures, including raised platforms and 90° plates. The angle of the attached plates can be controlled by varying the attachment point and cantilever tip's deflection. When compared to other methods of achieving these types of structures, buckled cantilevers are an attractive solution because they can be assembled with a simple mechanical motion. Furthermore, the cantilevers have a compliant connection to the substrate, which can be used for electrical routing.

Acknowledgments

We would like to gratefully acknowledge the support of the Natural Sciences and Engineering Research Council of Canada.

References

[1] Pister K S J, Judy M W, Burgett S R and Fearing R S 1992 Microfabricated hinges *Sensors Actuators* A **33** 249–56
[2] Lin L Y, Lee S S, Wu M C and Pister K S J 1995 Micromachined integrated optics for free-space interconnections *Proc. IEEE Micro Electro Mechanical Systems (MEMS '95)* pp 77–82
[3] Wu M C 1997 Micromachining for optical and optoelectronic systems *Proc. IEEE* **85** 1833–56
[4] Lin L Y, Goldstein E L and Tkach R W 1998 Free-space micromachined optical switches with submillisecond switching time for large-scale optical crossconnects *IEEE Photon. Technol. Lett.* **10** 525–7
[5] Young D J, Malba V, Ou J-J, Bernhardt A F and Boser B E 1997 Monolithic high-performance three-dimensional coil inductors for wireless communication applications *Technical Digest, Int. Electron Devices Meeting* pp 67–70
[6] Tien N C, Solgaard O, Kiang M H, Daneman M, Lau K Y and Muller R S 1996 Surface-micromachined mirrors for laser-beam positioning *Sensors Actuators* A **52** 76–80
[7] Reid J R, Bright V M and Comtois J H 1997 Automated assembly of flip-up micromirrors *Int. Conf. on Solid State Sensors and Actuators* vol 1 pp 347–50
[8] Dechev N, Cleghorn W L and Mills J K 2002 Micro-assembly of microelectromechanical components into 3-d mems *Can. J. Electr. Comput. Eng.* **27** 7–15
[9] Tsui K, Geisberger A A, Ellis M and Skidmore G H 2004 Micromachined end-effector and techniques for directed mems assembly *J. Micromech. Microeng.* **14** 542–9
[10] Dechev N, Cleghorn W L and Mills J K 2004 Microassembly of 3-d microstructures using a compliant, passive microgripper *J. Microelectromech. Syst.* **13** 176–89
[11] Tsang S H, Sameoto D, Foulds I, Leung A M and Parameswaran M 2006 Wirebonder assembly of hingeless 90° out-of-plane microstructures *Proc. Hilton Head 2006* pp 344–7
[12] Tsang S-H, Sameoto D and Parameswaran M 2006 Out-of-plane electrothermal actuators in silicon-on-insulator technology *Canadian Conf. on Electrical and Computer Engineering (CCECE 2006)* pp 97–103
[13] Tsang S-H, Sameoto D, Foulds I G, Johnstone R W and Parameswaran M 2007 Automated assembly of hingeless 90° out-of-plane microstructures *J. Micromech. Microeng.* **17** 1314–25
[14] Kaajakari V and Lal A 2003 Thermokinetic actuation for batch assembly of microscale hinged structures *J. Microelectromech. Syst.* **12** 425–32
[15] Syms R R A and Yeatman E M 1993 Self-assembly of 3-dimensional microstructures using rotation by surface-tension forces *Electron. Lett.* **29** 662–4
[16] Green P W, Syms R R A and Yeatman E M 1995 Demonstration of three-dimensional microstructure self-assembly *J. Micromech. Microeng.* **4** 170–6
[17] Syms R R A 1999 Surface tension powered self-assembly of 3-d micro-optomechanical structures *J. Microelectromech. Syst.* **8** 448–55
[18] Harsh K F, Bright V M and Lee Y C 1999 Solder self-assembly for three-dimensional microelectromechanical systems *Sensors Actuators* A **77** 237–44
[19] Syms R R A, Yeatman E M, Bright V M and Whitesides G M 2003 Surface tension-powered self-assembly of micro structures—the state-of-the-art *J. Microelectromech. Syst.* **12** 387–417
[20] Kubota K, Fleischmann T, Saravanan S, Vaccaro P O and Aida T 2003 Self-assembly of microstage using micro-origami technique on gaas *Japan. J. Appl. Phys.* 1 **42** 4079–83
[21] Ocampo J M Z *et al* 2003 Optical actuation of micromirrors fabricated by the micro-origami technique *Appl. Phys. Lett.* **83** 3647–9
[22] Li L, Zawadzka J and Uttamchandani D 2004 Integrated self-assembling and holding technique applied to a 3-d mems variable optical attenuator *J. Microelectromech. Syst.* **13** 83–90
[23] Johnstone R W, Sameoto D and Parameswaran M 2006 Non-uniform residual stresses for parallel assembly of out-of-plane surface-micromachined structures *J. Micromech. Microeng.* **16** N17–22
[24] Garcia E J 1998 Micro-flex mirror and instability actuation technique *Proc. 11th Ann. Int. Workshop on Micro Electro Mechanical Systems (MEMS 98)* pp 470–5
[25] Sameoto D, Ma A H, Parameswaran M and Leung A M 2007 Assembly and characterization of buckled cantilever platforms for thermal isolation in a polymer micromachining process *Canadian Conf. on Electrical and Computer Engineering (CCECE 2007)* pp 296–9
[26] Timoshenko S P and Gere J M 1961 *Theory of Elastic Stability* (New York: McGraw-Hill)
[27] Howell L L 2001 Compliant mechanisms *Chapter Flexibility and Deflection* (New York: Wiley)
[28] Conejo A J, Castillo E, Minguez R and Garc'ia-Bertrand R 2006 *Decomposition Techniques in Mathematical Programming* (Berlin: Springer)
[29] Koester D, Cowen A, Mahadevan R, Stonefield M and Hardy B 2003 *PolyMUMPs Design Handbook, Rev. 10* (Bernin: MEMSCAP)
[30] Bagdahn J, Sharpe W N and Jadaan O 2003 Fracture strength of polysilicon at stress concentrations *J. Microelectromech. Syst.* **12** 302–12
[31] Sharpe W N, Jackson K M, Hemker K J and Xie Z L 2001 Effect of specimen size on Young's modulus and fracture strength of polysilicon *J. Microelectromech. Syst.* **10** 317–26